Analysis of lattice Boltzmann nodes initialization in Moving Boundary problems

A. Caiazzo
Fraunhofer ITWM,
Fraunhofer-Platz, 1, D-67663 Kaiserslautern, Germany
E-mail: caiazzo@itwm.fhg.de

Abstract: The lattice Boltzmann method is a numerical scheme based on a fixed grid. Dealing with moving boundary problems, proper routines are needed to initialize the variables at the new nodes, created by the variations of the computational fluid domain. We use the asymptotic analysis to investigate the problem and possible solutions. A simple algorithm is proposed, able to achieve the same accuracy as the standard LBM. The theoretical predictions are tested on simple benchmarks.

Keywords: lattice Boltzmann equation, lattice Boltzmann initialization, asymptotic analysis.

1 INTRODUCTION

The lattice Boltzmann method (LBM) (Benzi et al., 1992; McNamara and Zanetti, 1988; Succi, 2001; Yu et al., 2003) is an approximate solver for the incompressible Navier-Stokes equations which discretizes the hydrodynamic problem using a kinetic model, based on a *fixed lattice*. Dealing with *moving boundaries*, the standard scheme has to be completed with an additional algorithm to initialize the variables on the nodes created by the variations of the computational domain.

Compared to other numerical methods, the LBM achieves needs a higher number of discrete variables. The additional need of resource is compensated by the simple formulation and by the favorable implementation. Therefore, the aim of the additional algorithm is to preserve the global efficiency and initialize the variables without spoiling the accuracy of the standard scheme.

Recently, LB algorithms to deal with moving boundary have been proposed and numerically tested (Lallemand and Luo, 2003; Ginzburg and d'Humiéres, 2003). In this work we use the asymptotic analysis to understand the problem in depth. Starting from a basic example, we show how a reliable algorithm can be constructed in a simple way.

In section 2 we introduce the lattice Boltzmann method, a moving boundary model problem and the main results of the asymptotic analysis for the standard scheme. In section 3 we focus on the refill step. A first approach (Lallemand and Luo, 2003) is described and tested. Performing the asymptotic expansion we prepare the basis for an improved refill algorithm (based on a similar idea proposed by Guo et al. (2002) to implement the boundary condition), which is discussed and numerically investigated in section 4.

2 LBM AND MOVING BOUNDARY PROBLEMS

As a model problem, we consider the motion of a solid disk in a two-dimensional domain. Formally, we divide a set $\Omega \subset \mathbb{R}^2$ as

$$\Omega = \Omega_F(t) \cup \Gamma(t) \cup \Omega_S(t), \tag{1}$$

in a fluid part $\Omega_F(t)$, a solid part $\Omega_S(t) = \{\mathbf{x} \in \Omega \mid \|\mathbf{x} - \mathbf{x}_C(t)\| < R\}$ and the interface Γ between them (fig. 1). We consider a solid domain to be a *rigid body* moving with prescribed motion, i.e. $\Omega_S(t)$ is a given function of time (*moving boundary problem without interaction*).

The fluid domain. In the fluid sub-domain, we consider the incompressible Navier-Stokes equations

$$\begin{cases} \nabla \cdot \mathbf{u} = 0 & t > 0,\ \mathbf{x} \in \Omega_F(t) \\ \partial_t \mathbf{u} + \nabla p + \mathbf{u} \cdot \nabla \mathbf{u} = \nu \Delta \mathbf{u} + \mathbf{G} & t > 0,\ \mathbf{x} \in \Omega_F(t) \end{cases}$$
$$\mathbf{u}(t, \mathbf{x}) = \mathbf{u}_B(t, \mathbf{x}) \quad t > 0,\ \mathbf{x} \in \Gamma(t) \cup (\partial\Omega \cap \partial\Omega_F(t))$$
$$\mathbf{u}(0, \mathbf{x}) = \mathbf{u}_0(\mathbf{x}) \quad \mathbf{x} \in \Omega_F(0), \tag{2}$$

where $\mathbf{u}_0$ is the initial velocity field of the fluid and $\mathbf{u}_B(t, \mathbf{x})$ is the prescribed velocity at the fluid-solid interface.

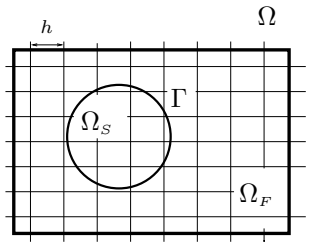

Figure 1: Moving boundary model problem: sketch of the domains introduced in equation (1) for the moving boundary model problem, discretized by a grid of type (4).

Alternatively, a Stokes problem can be taken into account, neglecting the non-linear term $\mathbf{u}\cdot\nabla\mathbf{u}$ in the previous system (2).

The hydrodynamics in $\Omega_F(t)$ is solved using the lattice Boltzmann method, which discretizes equation (2) starting from a *finite velocity Boltzmann equation*

$$\partial_t f_i(t,\mathbf{x}) + \mathbf{c}_i \cdot \nabla f_i(t,\mathbf{x}) = J_i(f(t,\mathbf{x})), \quad i = 1,\dots,b\,. \tag{3}$$

In equation (3), $\mathbb{V} = \{\mathbf{c}_i \mid i = 1,\dots,b\}$ is the finite velocity set and $f_i(t,\mathbf{x})$ represents the mass density distribution of the particles moving in direction $\mathbf{c}_i$, at time t and position $\mathbf{x}$. In this work we consider the D2Q9 discrete velocity model, depicted in fig. 2a. On the right hand side of equation (3), the collision operator $J_i(f)$ models the effect of the collisions between particles, which produce the variations in the distributions.

The domain is discretized in space with a regular h-grid

$$\mathcal{G}(h) = \left\{\mathbf{j} \in \mathbb{Z}^2 \mid \mathbf{x}_\mathbf{j} = h\mathbf{j} \in \Omega\right\} \tag{4}$$

and in time choosing the time step[a] $\Delta t = h^2$.

The LBM is described using a *dimensionless lattice units reference system*, denoting the numerical result at time $t_n = nh^2$ and at position $\mathbf{x}_\mathbf{j} = \mathbf{j}h$ through the function $\hat{f}_{ih}(n,\mathbf{j}) : \mathbb{N}\times\mathcal{G}(h) \to \mathbb{R}$. Using the BGK approximation for the collision operator J_i on the right hand side of (3), the general iteration of the algorithm reads (omitting the subscript h in $\hat{f}$)

$$\hat{f}_i(n+1,\mathbf{j}+\mathbf{c}_i) = \hat{f}_i(n,\mathbf{j}) + \frac{1}{\tau}(f_i^{eq}(\hat{f}) - \hat{f}_i)(n,\mathbf{j}) + g_i(n,\mathbf{j}). \tag{5}$$

The *equilibrium distribution* f^{eq} is a function of $\hat{f}$, through the local density $\hat{\rho} = \sum_i \hat{f}_i$ and the local velocity $\hat{\mathbf{u}} = \sum_i \mathbf{c}_i\hat{f}_i$ related to the distribution $\hat{f}$ at a lattice node:

$$f_i^{eq}(f) = H_i^{eq}\left(\rho(f), \mathbf{u}(f)\right), \tag{6}$$

where (for the D2Q9 model)

$$H_i^{eq}(\rho,\mathbf{u}) = f_i^*\left(\rho + c_s^{-2}\mathbf{c}_i\cdot\mathbf{u} + \frac{c_s^{-4}}{2}\left(|\mathbf{c}_i\cdot\mathbf{u}|^2 - c_s^2\mathbf{u}^2\right)\right). \tag{7}$$

[a]The relation $\Delta t = \Delta x^2$, called *diffusive scaling*, is a prerequisite to recover the incompressible Navier-Stokes equations in the limit Junk et al. (2005).

The lattice sound speed c_s and the weights f_i^* are model dependent (see for example Succi (2001) for detailed overview and descrptions of the method).

Using the LBM to solve a Stokes problem, only the linear part of the equilibrium function has to be considered.

Equation (5) expresses a relaxation towards the equilibrium distribution with a *single relaxation time* τ, related to a dimensionless viscosity through $\nu = c_s^2(\tau - \frac{1}{2})$. The additional term g_i is used to include the volume force:

$$g_i(n,\mathbf{j}) = c_s^{-2}h^3 f_i^*\mathbf{c}_i\cdot\mathbf{G}(t_n,\mathbf{x}_\mathbf{j}). \tag{8}$$

The implementation of algorithm (5) is usually split in two sub-steps, introducing the *post-collision* distributions

$$\hat{f}_i^C(n,\mathbf{j}) = \hat{f}_i(n,\mathbf{j}) + \frac{1}{\tau}(f_i^{eq}(\hat{f}) - \hat{f}_i)(n,\mathbf{j}) + g_i(n,\mathbf{j}), \tag{9}$$

and the *propagation step*

$$\hat{f}_i(n+1,\mathbf{j}+\mathbf{c}_i) = \hat{f}_i^C(n,\mathbf{j}). \tag{10}$$

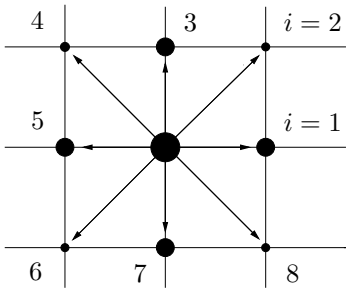

Figure 2: The D2Q9 discrete velocity model. Bigger circles correspond to larger weights f_i^*.

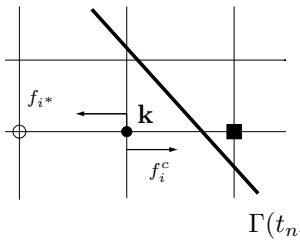

Figure 3: The BFL boundary conditions (11). The incoming population $f_{i^*}(n+1,\mathbf{k})$ has to be defined.

Boundary Conditions. If a fluid node $\mathbf{k} \in \mathcal{G}(h)$ has a neighbor $\mathbf{k}+\mathbf{c}_i$ in the solid domain the rule (10) cannot be used. In this case, we call $\mathbf{k}$ a *boundary node*, and $\mathbf{c}_i$ an *outgoing* direction in $\mathbf{k}$. We use the BFL algorithm (Bouzidi et al., 2001) to update the population at the boundary nodes (on the incoming link $\mathbf{c}_{i^*} = -\mathbf{c}_i$), according to the Dirichlet boundary condition of problem (2). It is based on a first order interpolation for the unknown distributions

(see figure 3):

$$\hat{f}_{i^*}(n+1,\mathbf{k}) = \begin{cases} 2q\hat{f}_i^C(n,\mathbf{k}) + (1-2q)\hat{f}_i^C(n,\mathbf{k}-\mathbf{c}_i) & q \le \frac{1}{2} \\ \quad +2c_s^{-2} f_i^* \mathbf{c}_i \cdot \mathbf{u}_B & \\ \frac{1}{2q}\hat{f}_i^C(n,\mathbf{k}) + (1-\frac{1}{2q})\hat{f}_{i^*}^C(n,\mathbf{k}) & q > \frac{1}{2} \\ \quad +\frac{1}{q}c_s^{-2} f_i^* \mathbf{c}_i \cdot \mathbf{u}_B & \end{cases} \tag{11}$$

where $q \in [0,1)$ is the node-boundary distance along the link $\mathbf{c}_i$ and $\mathbf{u}_B$ is evaluated at the point where the outgoing direction intersects the boundary.

Solid motion and Force Evaluation. We assume the motion of the solid domain to be given. Since the LBM is implemented only on the fluid nodes, according to $\Omega_S(t)$, at each time iteration we have to identify which nodes of the grid belong to the fluid domain. Additionally, in the numerical simulation the forces due to the fluid flow are evaluated using the *Momentum Exchange algorithm* (proposed in Ladd (1994)), which approximates the total boundary interaction with first order accuracy (Caiazzo and Junk, 2007). However, the topic is not treated in detail here.

A benchmark: Disk in incompressible Stokes flow. We construct an analytical solution to problem (2) (Stokes variant), considering the velocity field (G.Galdi, 1998)

$$\begin{aligned} u(t,x,y) &= U\left(\log\left(\xi(x,t)^2+\eta(y)^2\right) + \frac{2\eta(y)^2}{\xi(t,x)^2+\eta(y)^2} + \right. \\ &\qquad \left. \frac{\xi(t,x)^2-\eta(y)^2}{\left(\xi(t,x)^2+\eta(y)^2\right)^2}\right) \\ v(t,x,y) &= -U\frac{2\xi(t,x)\eta(y)}{\xi(t,x)^2+\eta(y)^2}\left(1-\frac{1}{\xi(x,t)^2+\eta(y)^2}\right) \end{aligned} \tag{12}$$

and the pressure

$$p(t,x,y) = -\frac{4U\nu}{R}\frac{\xi(t,x)}{\xi(t,x)^2+\eta(y)^2}, \tag{13}$$

where

$$\xi(t,x) = \frac{x-(x_C^0+Ut)}{R},\ \eta(y) = \frac{y-y_C^0}{R} \tag{14}$$

are reference coordinates with respect to the center of the disk, moving horizontally with constant speed U (fig. 4).

Including the volume force

$$\mathbf{G}(t,x,y) = \partial_t \mathbf{u}(t,x,y) \tag{15}$$

and assigning the fields (12) as Dirichlet boundary conditions on the edge of a square $\Omega = [0,L]\times[0,L]$, u, v and p as defined in (12)-(13) solve the Stokes problem in Ω, where the solid disk $\Omega_S(t)$ moves along x with velocity U. For this flow field, the boundary force is

$$F = 8\pi\nu U. \tag{16}$$

We refer to this test problem as *Disk-in-Flow* (DiF). Moreover, by adding the constant horizontal speed $-U$ to (12), we define a *fixed boundary* variant of the problem, called DiF^0, whose exact horizontal velocity is now zero along the disk boundary, while v and p are the same as in (12)-(13).

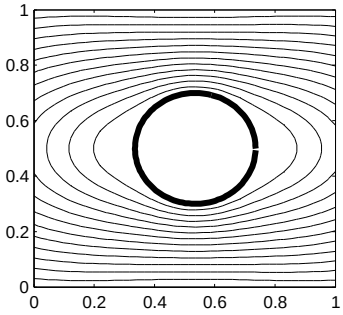

Figure 4: DiF benchmark. Streamlines of the velocity field (12). In the numerical simulation, we use a circle of radius $R = 0.6$ in a square box of edge length $L = 3$. Viscosity is $\nu = 0.03$.

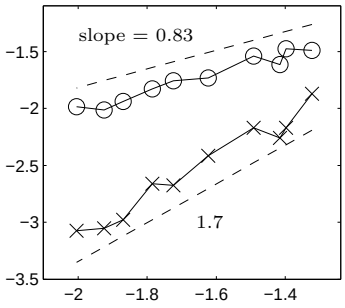

Figure 5: DiF benchmark. Double logarithmic plot of maximum error in pressure (circles ∘) and velocity (crosses ×) versus grid size for the benchmark DiF^0 (fixed boundary). The experimental orders of accuracy is given by the slope of the linear least squares approximation of the error data (dashed lines). It is close to the theoretical expectations, i.e. second order velocity and first order pressure.

Asymptotic Analysis To investigate the LB algorithm (Junk et al., 2005) we introduce an expansion of the numerical solution in power series of the small parameter h

$$\hat{f}_{ih}(n,\mathbf{j}) = f_i^{(0)}(t_n,\mathbf{x_j}) + hf_i^{(1)}(t_n,\mathbf{x_j}) + h^2 f_i^{(2)}(t_n,\mathbf{x_j}) + \dots, \tag{17}$$

where the coefficients are assumed to be smooth and depending on the physical time and space. To derive the functions $f_i^{(k)}$, we insert the expansion (17) into the algorithm (5) (and into (11) for the boundary nodes). Taylor expanding around $(t_n,\mathbf{x_j})$ and sorting the different orders in h, we obtain a set of partial differential equations for the coefficients, which are solved in the leading orders by

(Junk et al., 2005; Junk and Yang, 2005)

$$\begin{aligned} f_i^{(0)} &= f_i^*, \\ f_i^{(1)} &= f_i^* c_s^{-2} \mathbf{c}_i \cdot \mathbf{u}, \\ f_i^{(2)} &= f_i^* c_s^{-2} p + \frac{f_i^* c_s^{-4}}{2} \left(|\mathbf{c}_i \cdot \mathbf{u}|^2 - c_s^2 \mathbf{u}^2 \right) - \\ & \quad \tau f_i^* c_s^{-2} \mathbf{c}_i \cdot \nabla \mathbf{u} \cdot \mathbf{c}_i, \end{aligned} \tag{18}$$

$\mathbf{u}$ and p being a solution of Navier-Stokes (or Stokes, if only a linearized equilibrium is used) equation (2). Then, we analyze the numerical method using the *prediction*

$$F_{ih} = f_i^{(0)} + h f_i^{(1)} + h^2 f_i^{(2)}, \tag{19}$$

composed by equilibrium and non-equilibrium part (see equation (7)) :

$$\begin{aligned} F_{ih} &= H_i^{eq}(1 + h^2 c_s^{-2} p, h\mathbf{u}) - h^2 \tau f_i^* c_s^{-2} \mathbf{c}_i \cdot \nabla \mathbf{u} \cdot \mathbf{c}_i = \\ &= F_{i_h}^{EQ}(p, \mathbf{u}) + F_{i_h}^{NEQ}(\nabla \mathbf{u}). \end{aligned} \tag{20}$$

Since we can extract the Navier-Stokes solution taking suitable moments of F_h, we conclude that the corresponding moments of the numerical solution $\hat{f}_h$ yield

$$\begin{aligned} h^{-1}\hat{\mathbf{u}} &= \frac{\sum_i \mathbf{c}_i \hat{f}_{ih}}{h} = \mathbf{u} + O(h^2), \\ \hat{p} &= c_s^2 \frac{\sum_i \hat{f}_{ih} - 1}{h^2} = p + O(h), \end{aligned} \tag{21}$$

i.e. a second order accurate velocity and a first order accurate pressure. Additionally, we can approximate the viscous stress tensor from the *non-equilibrium* part:

$$\begin{aligned} \hat{\mathbf{S}}[\mathbf{u}] &= -\frac{\nu}{c_s^2 \tau h^2} \sum_i \mathbf{c}_i \otimes \mathbf{c}_i \left(\hat{f}_i - f_i^{eq}(\hat{f}) \right) = \\ &= \nu \left(\nabla \mathbf{u} + \nabla \mathbf{u}^T \right) + O(h). \end{aligned} \tag{22}$$

The numerical results for the fixed boundary case DiF^0 (fig. 5) validate the theoretical prediction for the accuracy of the standard LBM.

3 THE REFILL PROBLEM

Let us focus now on a moving boundary problem. Namely, let $\mathbf{k}$ be a node such that $\mathbf{x_k} \in \Omega_S(t_n)$ and $\mathbf{x_k} \in \Omega_F(t_{n+1}) \cup \Gamma(t_{n+1})$, i.e. $\mathbf{x_k}$ enters the fluid domain at time t_{n+1}. We need to *refill* the new fluid point, initializing the variables $\hat{f}_i(n+1, \mathbf{k})$. The missing information has to be recovered from the neighboring nodes. Since the main properties of the LBM are the favorable implementation (9)+(10) and the reliability for parallel computing, the effort needed to perform refill steps becomes relevant for the global efficiency. Mainly, the additional algorithm should not require an excessive amount of *exchange of information* and be *well fitting* in the LB structure.

Example: The equilibrium refill We start analyzing a simple approach (Lallemand and Luo, 2003), which reconstructs the populations using the equilibrium distribution for approximate density and velocity.

Let $\mathbf{k} \in \mathcal{G}(h)$ the node to be refilled at time step $n+1$. We compute first $\tilde{\rho}_{n+1,\mathbf{k}}$ and $\tilde{\mathbf{u}}_{n+1,\mathbf{k}}$, approximations of density and velocity at $\mathbf{k}$, defining then the *equilibrium refill*:

$$\hat{f}_i(n+1, \mathbf{k}) = H_i^{eq}(\tilde{\rho}_{n+1,\mathbf{k}}, \tilde{\mathbf{u}}_{n+1,\mathbf{k}}). \tag{23}$$

The particular choice of the extrapolation rule for $\tilde{\rho}$ and $\tilde{\mathbf{u}}$ might depend on the considered flow and motion of the boundary. For example, we can use a backward extrapolation according to the boundary velocity $\mathbf{u}_B$ at a point of interface close to the new node (Lallemand and Luo, 2003).

Numerical tests. The equilibrium refill is now applied to problem DiF. Figure 6 shows the maximum error in pressure over $\Omega_F(t)$ versus time. The peaks appearing in correspondence to the refill steps do not decrease on the finer grid. In the order plot in fig. 7 the errors for different grid sizes are compared. We observe a first order accuracy for the velocity but an inconsistent pressure (the error does not decrease using a finer discretization).

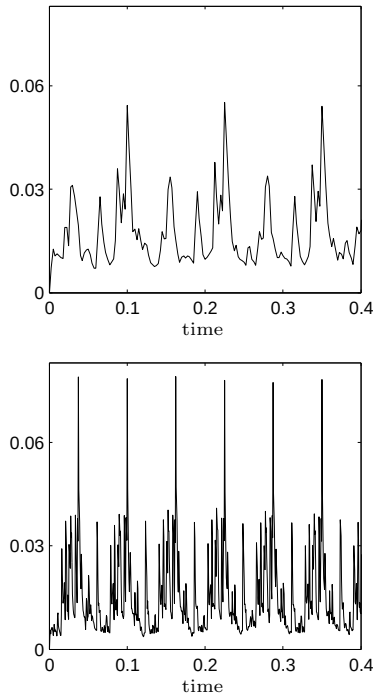

Figure 6: DiFBenchmark . Error in pressure (maximum over $\Omega_F(t)$) using the algorithm (23) to initialize the new nodes. Grid sizes $h = 0.05$ (top) and $h = 0.025$ (bottom) are shown.

Asymptotic analysis: prediction for the equilibrium refill. In the previous section, the coefficients (18) and the truncated expansion F_h have been derived considering the LBM (5) and the boundary rule (11). Using an additional algorithm to initialize the new node, the accuracy results (21) are not assured.

Applying the same procedure, we insert the expansion (17) into the algorithm (23), used at a new node $\mathbf{k}$. We

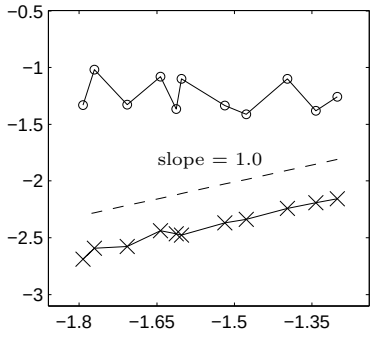

Figure 7: DiFbenchmark. Double logarithmic plot of maximum errors (in space and time) in pressure ($\circ$) and velocity ($\times$), versus grid size. The dashed curve shows a reference line of slope one. We get a first order accurate velocity and an inconsistent pressure.

find that the coefficient $f^{(2)}$ cannot be defined for the whole domain as in (18). Not surprisingly, using the equilibrium refill the *non-equilibrium part* (in the second order)

$$f_i^{neq,(2)} = -\tau f_i^* c_s^{-2} \mathbf{c}_i \cdot \nabla \mathbf{u} \cdot \mathbf{c}_i \tag{24}$$

will be missing at the new refilled point. As a consequence, the prediction (19) and the related accuracy results are no longer justified.

Remarks. Observe that we could reduce to the truncated expansion

$$G_{ih} = f^{(0)} + h f^{(1)} \tag{25}$$

which predicts a first order accurate velocity and does not contains information about pressure and stress tensor. Although the equilibrium refill approximates accurately the hydrodynamics on the new node, the lack of non equilibrium also spoils the accuracy in pressure and velocity during the time iterations.

In previous works (Lallemand and Luo, 2003; Ginzburg and d'Humiéres, 2003) algorithms able to achieve the LB accuracy have also been proposed. However, the knowledge acquired with the analysis allows us to solve the problem constructing a simple scheme.

4 NON-EQUILIBRIUM CORRECTION

According to the analysis, all we need to keep the scheme as accurate as the interior LBM is a refill step able to reconstruct *equilibrium and non equilibrium* with enough accuracy.

We complete the initialization of the populations (23) including an approximation of the non equilibrium part by a first order extrapolation, simply *copying* the non equilibrium part from a neighbor of the new fluid node[b]. It has to be mentioned that a similar idea was used in Guo et al. (2002), to implement the Dirichlet boundary condition. In practice, we propose the following algorithm to refill the node $\mathbf{k}$.

- choose a (flow depending) extrapolation direction $\mathbf{c}_i^{ex}$ (not outgoing at $\mathbf{k}$)
- compute approximations $\tilde{\rho}_{n+1,\mathbf{k}}$, $\tilde{\mathbf{u}}_{n+1,\mathbf{k}}$
- *equilibrium + non equilibrium* refill:

$$\begin{aligned} \hat{f}_j(n+1,\mathbf{k}) = H_j^{eq}\left(\tilde{\rho}_{n+1,\mathbf{k}}, \tilde{\mathbf{u}}_{n+1,\mathbf{k}}\right) + \\ f_j^{neq}(n+1, \mathbf{k}+\mathbf{c}_i^{ex}), \quad j = 1,\ldots,b. \end{aligned} \tag{26}$$

Simulating the problem DiF, we observe (fig. 8 and fig. 9) improvements in accuracy, which is now comparable with the accuracy of the standard LBM.

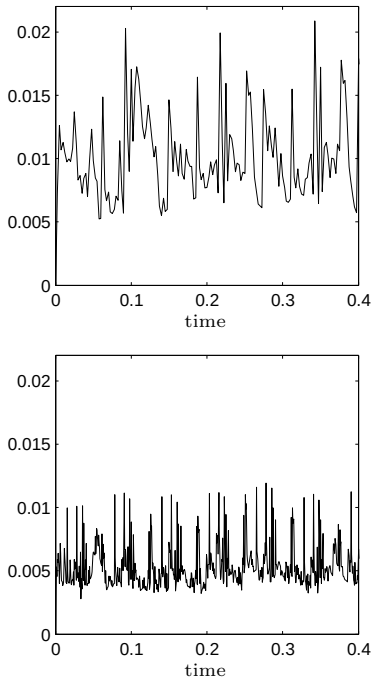

Figure 8: Results for the benchmark DiF employing the non-equilibrium corrected refill. Maximum error in pressure over $\Omega_F(t)$, $h = 0.05$ (top) and $h = 0.025$ (bottom). Unlike in the previous test case, now the results improve on the finer grid.

Force investigations As remarked concluding the analysis (end of section 3), the lack of non equilibrium part affects the *pressure* and the *stress tensor* at the nodes close to the interface (where the refills take place), which are contained in the second order part of the numerical solution. In other words, the error might influence directly the computation of the boundary forces. Figures 10 and 11 show the error in the horizontal force (exact solution (16)). Using the non-equilibrium correction we obtain better results.

[b] Due to the poor accuracy (first order in pressure) of the LBM, using a higher order extrapolation does not lead theoretically to better results.

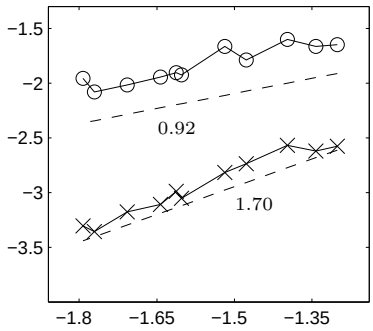

Figure 9: Double logarithmic plot of the maximum errors in pressure (∘) and velocity (×) versus grid size (benchmark DiF, including the non-equilibrium correction). The slopes of the straight approximations (dashed lines) are also indicated.

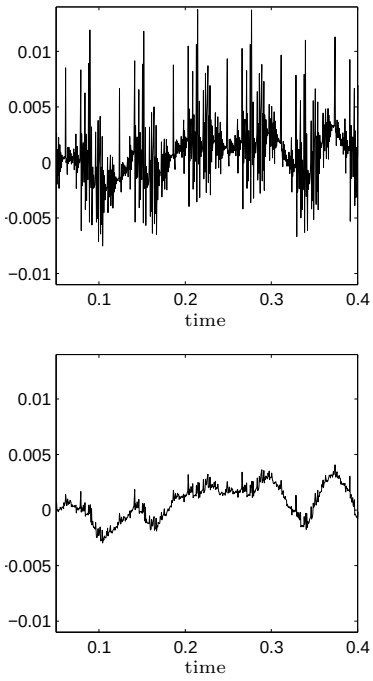

Figure 10: Top: Error in horizontal force (problem DiF), using the equilibrium refill. Grid size $h = 0.025$. Bottom: Non-equilibrium correction is included.

We compare the two approaches on a further benchmark (depicted in fig. 12), based on a *full Navier-Stokes* problem. A disk moves horizontally in a periodic channel, with velocity approaching a stationary regime. We refer to this problem as DiF_2.

At the steady state, we obtain a physically equivalent problem keeping the disk fixed and moving the channel walls in the opposite direction (Galilean invariance). To investigate the influence of the refill steps on the force computation we compare the drag forces on the disk in the two cases (fig. 13), looking at the difference $\Delta_F(t) = \left|F^{MOV} - F^{FIX}\right|$, where F^{MOV} and F^{FIX} are the forces

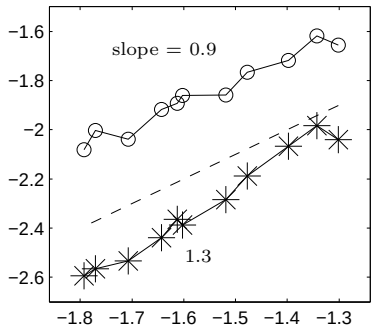

Figure 11: Double logarithmic plot of error versus grid size for the force computation. ∘: EQ refill. ×: EQ + non-EQ. Including the non-equilibrium correction the errors decreases faster. Dashed line: reference line of slope 1 (first order accuracy).

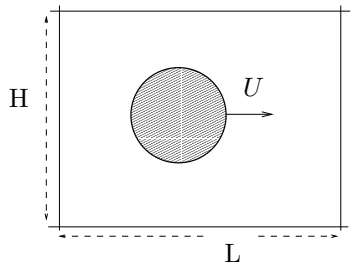

Figure 12: Benchmark DiF_2. A disk (radius $R = 0.2$) moves horizontally in a channel of unitary length ($L = H = 1$), with periodic boundary in x-direction, reaching a stationary velocity $u = 1$. Viscosity is $\nu = 0.03$.

obtained in the two different reference systems (with *moving* and resp. *fixed* disk).

The two problems give similar stationary results. In detail, we observe that the refill steps produce a series of jumps in the force. Using the non-equilibrium corrected refill the size of the peaks and the discrepancy in the forces reduce (first order in h, figures 14, 15). As in the previous test, the accuracy is in general better than the one observed for the simpler equilibrium refill.

Conclusive remarks. The non-equilibrium corrected refill improves the results, both in terms of order of accuracy and size of the errors, compared to the simpler equilibrium one. In both cases the error shows an irregular profile, charachterized by jumps appearing in correspondence to the refills (due to the sudden switching on of fluid nodes). It has to be remarked that the irregularity in the numerical results might affect the validity of the conclusions obtained by a *regular asymptotic expansion* (17). Nevertheless, the analysis is still an useful tool which can be used to understand the algorithms, to detect where and how the errors originate and how to construct corrected schemes.

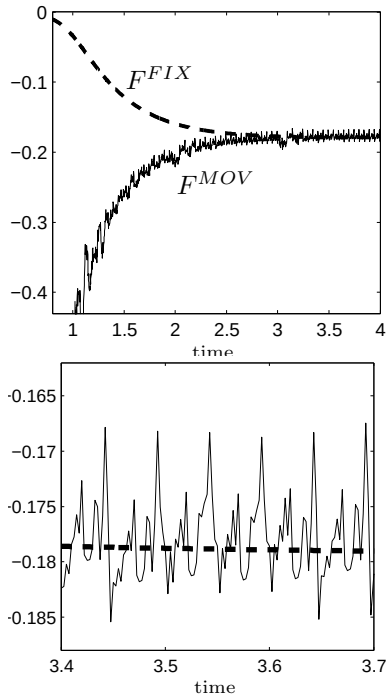

Figure 13: Values of the drag force on the moving disk (F^{MD}), simulating the problem DiF_2 in the disk reference system (F^{FIX}). Grid size $h = \frac{1}{20}$. On the right, the zoom on a small time interval evidences the oscillations in the results.

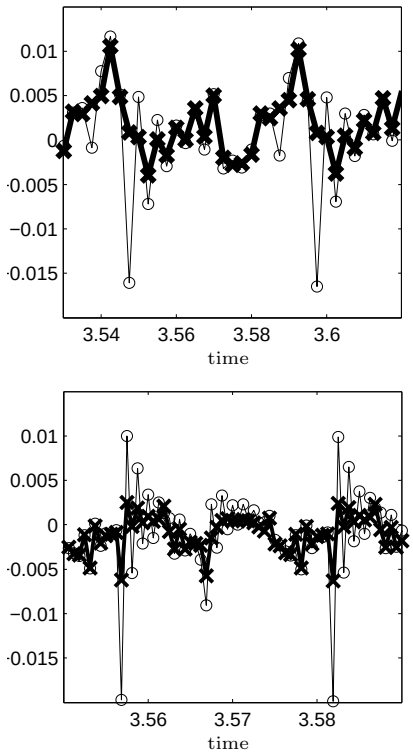

Figure 14: Difference $\Delta_F(t)$. ∘: EQrefill, ×: EQ+non EQ refill. Comparisons of the jumps affecting the results, grids $h = \frac{1}{20}$ (top) and $h = \frac{1}{40}$ (bottom).

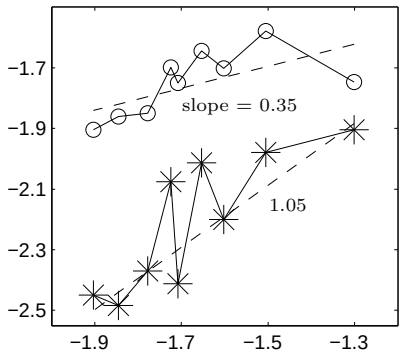

Figure 15: Double logarithmic plot of the maximum in time of $\Delta_F(t)$ versus the grid size h. ∘: EQrefill, ×: EQ+non EQ refill. In both the cases the errors are strongly oscillating.

REFERENCES

Benzi, R., Succi, S., and Vergassola, M. (1992). The lattice boltzmann equation: Theory and applications. *Phys. Rep.*, 222:147–197.

Bouzidi, M., Firdaouss, M., and Lallemand, P. (2001). Momentum transfer on a boltzmann lattice fluid with boundaries. *Physics of Fluids*, 13:3452–3459.

Caiazzo, A. and Junk, M. (2007). Boundary forces in lattice Boltzmann: analysis of Momentum Exchange algorithm. *To appear on Computer and Mathematics with Applications*.

G.Galdi (1998). *An Introduction to the Mathematical Theory of the Navier-Stokes Equation (Volume 1)*. Springer-Verlag.

Ginzburg, I. and d'Humiéres, D. (2003). Multireflection boundary conditions for lattice boltzmann models. *pre*, 68:066614.

Guo, Z., Zheng, C., and Shi, B. (2002). An extrapolation method for boundary conditions in lattice boltzmann method. *Physics of Fluid*, 14:2007–2010.

Junk, M., Klar, A., and Luo, L.-S. (2005). Asymptotic analysis of the lattice Boltzmann Equation. *Journal Comp. Phys.*, 210:676–704.

Junk, M. and Yang, Z. (2005). A one-point boundary condition for the lattice Boltzmann method. *submitted*.

Ladd, A. J. C. (1994). Numerical simulations of particular suspensions via a discretized boltzmann equation. part 1. *J. Fluid Mech.*, 271:285–310.

Lallemand, P. and Luo, L.-S. (2003). Lattice boltzmann method for moving boundaries. *J. Comp. Phys.*, 184:406–421.

McNamara, G. and Zanetti, G. (1988). Use of the boltzmann equation to simulate lattice-gas automata. *Phys. Rew. Lett.*, 61:2332–2335.

Succi, S. (2001). *The Lattice Boltzmann Equation for Fluid Dynamics and Beyond*. Oxford University Press.

Yu, D., Mei, R., Luo, L.-S., and Shyy, W. (2003). Viscous flow computation with the method of the lattice boltzmann equation. *Progress in Aerospace Sciences*, 39:329–367.